# Resonant instability of ducted free supersonic mixing layers induced by periodic Mach waves

# By CHRISTOPHER K. W. TAM AND FANG Q. HU

Department of Mathematics, Florida State University, Tallahassee, FL 32306-3027, USA

(Received 24 November 1989 and in revised form 18 January 1991)

It is known that the mixing or spreading rate of free mixing layers decreases with an increase in the convective Mach number of the flow. At supersonic convective Mach number the natural rate of mixing of the shear layers is very small. It is believed that the decrease in mixing rate is directly related to the decrease in the rate of growth of the instabilities of these flows. In an earlier study (Tam & Hu 1989) it was found that inside a rectangular channel supersonic free shear layers can support two families of instability waves and two families of acoustic wave modes. In this paper the possibility of driving these normal acoustic wave modes into resonant instability by using a periodic Mach wave system is investigated. The Mach waves can be generated by wavy walls. By properly choosing the wavelength of the periodic Mach wave system mutual secular excitation of two selected acoustic wave modes can be achieved. In undergoing resonant instability, the acoustic modes are locked into mutual simultaneous forcing. The periodic Mach waves serve as a catalyst without actually being involved in energy transfer. The resonant instability process is analysed by the method of multiple scales. Numerical results indicate that by using wavy walls with an amplitude-to-wavelength ratio of  $1\frac{1}{2}\%$  it is possible to obtain a total spatial growth of e9 folds over a distance of ten channel heights. This offers reasonable promise for mixing enhancement. The results of a parametric study of the effects of flow Mach numbers, temperature ratio, shear-layer thickness, modal numbers as well as three-dimensional effects on the spatial growth rate of the resonant instability are reported and examined so as to provide basic information needed for future feasibility analysis.

#### 1. Introduction

Recent investigations by Ikawa & Kubota (1975), Bogdanoff (1983), Papamoschou & Roshko (1986, 1988) and Chinzei et al. (1986) have established experimentally that the mixing or spreading rate of supersonic shear layers decreases as the convective Mach number increases. Papamoschou & Roshko were the first to demonstrate that there is a strong correlation between their measured spreading rate data (normalized by the incompressible flow value) and the theoretical maximum growth rate of the instability waves of the shear layer. Since then the theoretical instability wave growth curve has been recomputed and its good correlation with the experimental measurements reconfirmed by Ragab & Wu (1989), Zhuang, Kubota & Dimotakis (1988), and Jackson & Grosch (1989) using unconfined mixing-layer models. A more recent calculation by Zhuang, Kubota & Dimotakis (1989) using a shear-layer model enclosed at the top and bottom by solid walls essentially reproduces similar results. The implication of these works is that flow instability is the principal mechanism

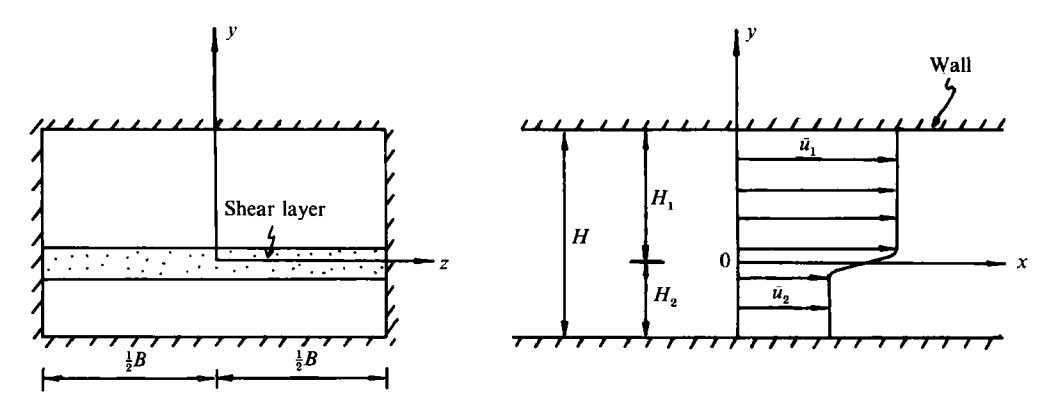
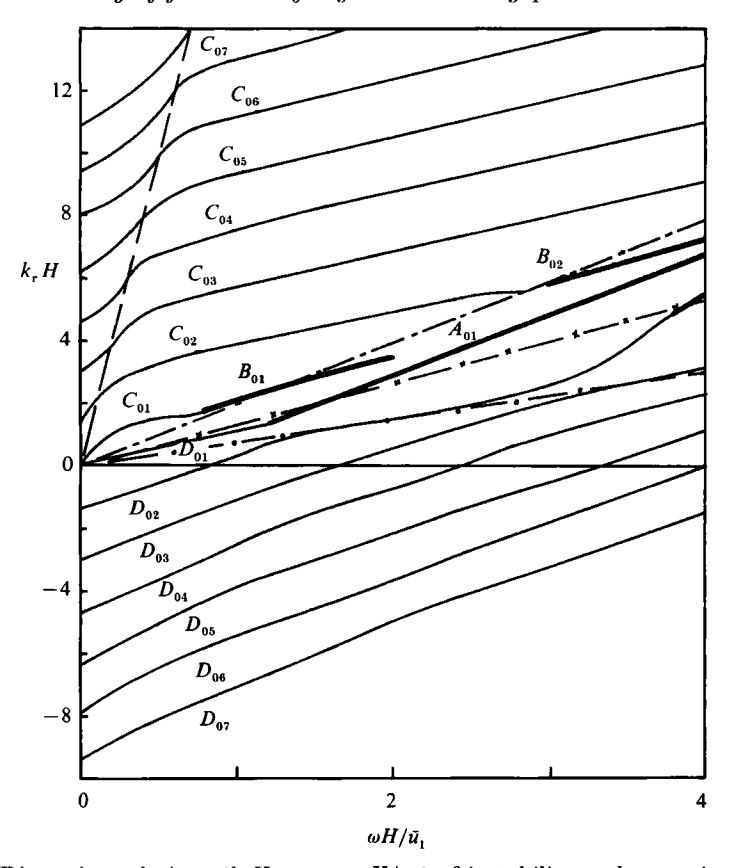


FIGURE 1. Free shear layer inside a rectangular channel.

responsible for the mixing and spreading of high-speed shear layers. Further, the decrease in the spreading rate of a supersonic mixing layer is due directly to the decrease in the growth rate of the inherent instability waves of the flow. In many practical problems such as shear flows inside the supersonic combustors of jet engines it is essential to have a large mixing rate. In the light of the recent experimental results it becomes apparent that the required mixing rate cannot be achieved by the natural instability and mixing processes. The primary objective of this paper is to investigate the feasibility of using a new mixing enhancement scheme. This scheme uses a periodic Mach wave system generated by a slight waviness of the enclosure surfaces. It will be shown below that the presence of a suitably chosen periodic Mach wave system induces the natural wave modes of the ducted shear flow to undergo resonant instability. Numerical results indicate that large enough instability growth rates can be realized, giving rise to the possibility of achieving a greatly enhanced rate of mixing.

It is now known that ducted free shear layers behave differently from their unconfined counterparts at high speeds. When housed inside a rectangular channel (see figure 1) the motion of a supersonic shear layer is invariably coupled to the acoustic modes of the duct. This coupled motion was studied recently by a number of investigators including Zhuang et al. (1989), Greenough et al. (1989), Mack (1989) and the present authors (Tam & Hu 1989). In our work an extensive search of the normal wave modes of the coupled motion was carried out. It was found that because of the coupling to the acoustic modes a thin shear layer which is known to become neutrally stable at high supersonic convective Mach number (see Miles 1958) remained unstable in the confined environment. Systematic calculations showed that for ducted supersonic shear layers there are two basic families of instability waves (the A and B modes). Each wave mode within each family is characterized by two integer mode numbers (m, n). The m-number is related to the number of reflections off the two sidewalls. The *n*-number is related to the number of reflections off the top and bottom walls of the channel. For clarity, members of the two families of instability waves are designated as  $A_{mn}$  and  $B_{mn}$  (m = 0, 1, 2, ...; n = 1, 2, 3, ...)respectively. Typical dispersion relations for a few of the lower-order modes of these instabilities at  $M_1$  (Mach number of the fast stream) = 3.5 and  $M_2$  (Mach number of the slow stream) = 1.2 with sound speed ratio  $a_1/a_2 = 1.2$  are shown in figure 2. For reference, the growth rates  $(-k_i H, \text{ where } H \text{ is the channel height) of the } A_{01} \text{ mode}$ at different ratios of the shear-layer vorticity thickness to channel height  $(\delta_{\omega}/H)$  as



functions of the non-dimensional angular frequency are provided in figure 3. It is readily seen from this figure that in a channel of fixed height the growth rate of the instability wave decreases rapidly with increase in shear-layer thickness. Over a reasonably long propagation distance, say ten channel heights, the total amplification of the instability waves is quite small; insufficient to bring about an adequate rate of mixing.

In addition to the two families of instability waves, two families of neutral acoustic modes were also identified (referred to as the C and D modes). The members of these two families of waves are also specified by two integer mode numbers (m,n) as in the case of the unstable waves. Again the m-number is related to the number of reflections off the sidewalls and the n-number is related to the number of reflections off the top and bottom walls. Typical dispersion relations of these  $C_{mn}$  and  $D_{mn}$  ( $m=0,1,2,\ldots; n=1,2,3,\ldots$ ) acoustic modes are shown in figure 2. It is to be noted that although the wavenumbers of the  $D_{mn}$  modes are negative at low frequencies they, like the  $C_{mn}$  modes, are downstream-propagating waves (see Tam & Hu 1989 for details).

We will now outline the basic idea of using a periodic Mach wave system to drive the natural wave modes of the flow into resonant instability. Since the flow is supersonic it is easy to introduce a periodic Mach wave system into the channel flow

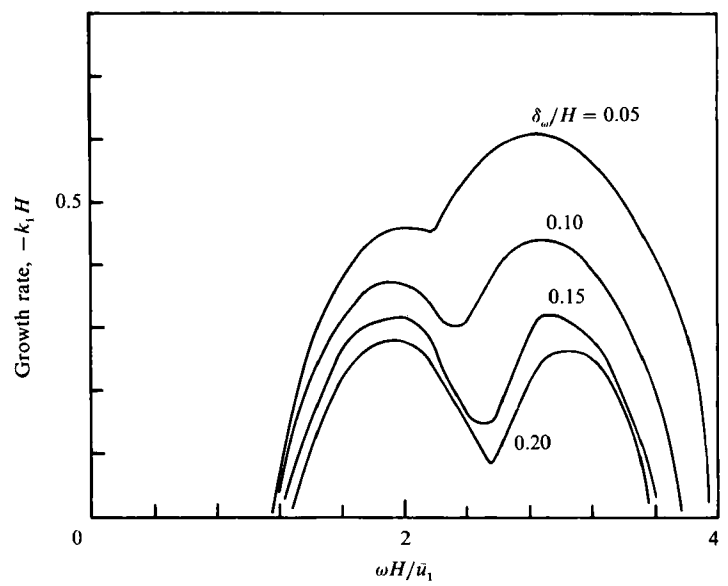


Figure 3. Growth rate of the  $A_{01}$  instability wave at different vorticity thicknesses.  $M_1=3.5$ ,  $M_2=1.2$ ,  $a_1/a_2=1.2$ ,  $\gamma_1=\gamma_2=1.4$ ,  $H_1=H_2=0.5H$ .

by making the top and bottom channel walls slightly wavy as shown in figure 4. Without loss of generality let us consider resonant instability involving a  $C_{mn}$  wave and a  $D_{mn'}$  wave of the same frequency  $\omega$ . For illustration, it will be assumed for the time being that all the waves are one-dimensional (the complete three-dimensional wave mode analysis is given in §3). The  $C_{mn}$  and  $D_{mn'}$  waves as well as the Mach waves may be represented mathematically by

$$C \operatorname{e}^{\mathrm{i}(k_C x - \omega t)}, \quad D \operatorname{e}^{\mathrm{i}(k_D x - \omega t)}, \quad A \cos{(k_M x)} = \tfrac{1}{2} A (\operatorname{e}^{\mathrm{i}k_M x} + \operatorname{e}^{-\mathrm{i}k_M x)},$$

where C and D are the wave amplitudes of the propagating waves and A is the amplitude of the standing periodic Mach waves.  $k_C$  and  $k_D$  are the wavenumbers of the  $C_{mn}$  and  $D_{mn'}$  waves respectively and  $k_M$  is the wavenumber of the Mach waves. Suppose the wavenumber of the Mach waves is chosen so that the resonance condition

$$k_C - k_D = k_M \tag{1}$$

is satisfied. As the  $C_{mn}$  and  $D_{mn'}$  waves propagate downstream through the Mach wave field they will invariably interact with the periodic wave system (through the nonlinear terms of the flow equations) giving rise to a set of non-homogeneous terms. Some of these terms arising from the interaction between the  $C_{mn}$  wave and the Mach waves have the form

$$C e^{i(k_C x - \omega t)} A e^{-ik_M x} = A C e^{i(k_D x - \omega t)};$$
(2)

(2) is in the form of a  $D_{mn'}$  wave. Similarly the interaction of the  $D_{mn'}$  wave and the Mach waves gives rise to product terms of the form,

$$D e^{i(k_D x - \omega t)} A e^{ik_M x} = AD e^{i(k_C x - \omega t)}, \tag{3}$$

which is in the form of a  $C_{mn}$  wave. The nonlinear product terms provide a forcing on the respective waves. Since the forcing functions have the same frequency and

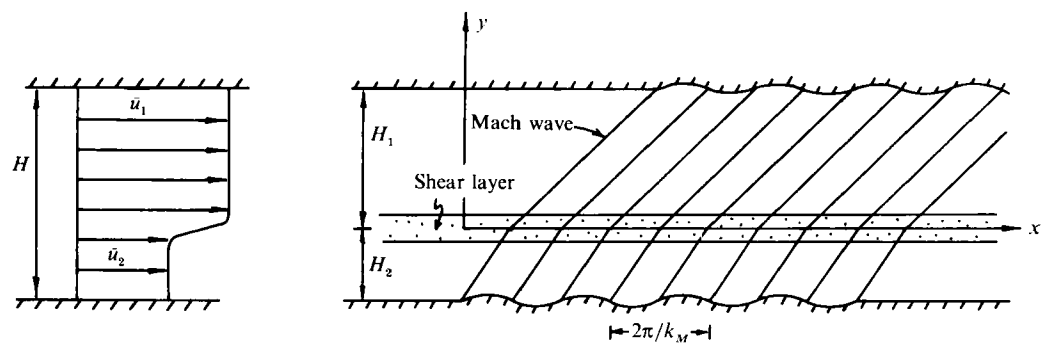


FIGURE 4. Periodic Mach waves generated by wavy walls inside a rectangular channel.

wavelength as the natural wave modes, resonance would occur. In the present context, the periodic Mach waves act as a catalyst allowing the  $C_{mn}$  wave to force the  $D_{mn'}$  wave and vice versa. In this way, as will be shown later, under mutual forcing the two waves grow exponentially as they propagate downstream, exhibiting the phenomenon of resonant instability.

It is worthwhile to point out that there are other examples in the literature involving strong resonances arising from the interaction of wave trains and a stationary periodic field. However, these resonances do not always lead to instabilities. Recently Mei and coworkers (Mei 1985; Mei, Hara & Naciri 1988) studied the resonance between water waves incident on periodic longshore sandbars. The phenomenon is analogous to Bragg reflection in crystallography. Strong resonant reflection was found. But there was no instability. On comparing the resonance mechanisms described by Mei and the above discussion it is noted that resonant instability could occur when two wave trains with matching wavenumbers with respect to the stationary periodic field are present. When there is one incident or forced wave train only resonant reflection could occur. The condition for resonant reflection is that the difference between the wavenumbers of the incident and the reflected waves is equal to that of the scatter field.

In §2 of this paper the mean flow profile and the periodic Mach wave field used in the instability analysis will be discussed. In §3 resonant instability of two normal wave modes of a ducted shear flow in the presence of a periodic Mach wave system if analysed using the method of multiple scales (see e.g. Nayfeh 1973). Typical numerical results are reported in §4. It turns out that the spatial growth rate of the resonant instability is dependent on a number of factors. They include the Mach numbers and the temperature ratio of the flow streams, the shear-layer thickness and the wave modes involved. The results of a parametric study of these effects are reported in §5. Finally a short discussion of the feasibility of using periodic Mach waves to induce resonant instability for mixing enhancement is given in the last section of this paper.

# 2. Mean flow and the periodic Mach waves

We will consider a two-dimensional shear layer inside a rectangular channel of height H and width B as shown in figure 1. For simplicity we will assume that the gases on the two sides of the mixing layer are the same and are inviscid and non-heat conducting. The fast stream on the top will be labelled by a subscript 1 and the slow

stream on the bottom will be labelled by a subscript 2. The continuity, momentum and energy equations for such a flow are

$$\frac{\partial \rho}{\partial t} + \nabla \cdot (\rho \mathbf{v}) = 0, \tag{4}$$

$$\rho\left(\frac{\partial \boldsymbol{v}}{\partial t} + \boldsymbol{v} \cdot \nabla \boldsymbol{v}\right) = -\nabla p,\tag{5}$$

$$\frac{\partial p}{\partial t} + \boldsymbol{v} \cdot \boldsymbol{\nabla} p + \gamma p \boldsymbol{\nabla} \cdot \boldsymbol{v} = 0, \tag{6}$$

where  $\gamma$  is the ratio of the specific heats of the gas. The time-independent solution of the above system of equations which satisfies the boundary conditions at the walls of the channel is

$$\mathbf{v} = \bar{u}(y)\,\hat{\mathbf{e}}_x, \quad \rho = \bar{\rho}(y), \quad p = \bar{p} = \text{const},$$
 (7)

where  $\hat{e}_x$  is the unit vector in the x-direction. In all the numerical work of this paper the mean velocity and density will be assumed to have hyperbolic tangent profiles. Specifically we will use

$$\bar{u} = \frac{1}{2} \left[ \bar{u}_1 + \bar{u}_2 + (\bar{u}_1 - \bar{u}_2) \tanh\left(\frac{2y}{\delta_\omega}\right) \right],\tag{8}$$

$$\bar{\rho} = \frac{1}{2} \left[ \bar{\rho}_1 + \bar{\rho}_2 + (\bar{\rho}_1 - \bar{\rho}_2) \tanh\left(\frac{2y}{\delta_{\omega}}\right) \right]. \tag{9}$$

In (8) and (9)  $\delta_{\omega}$  is the vorticity thickness of the shear layer. It is to be noted that with constant mean pressure the mean temperature distribution is proportional to the inverse of the density distribution. The hyperbolic tangent velocity profile (8) is a reasonably good approximation of the velocity profiles measured by Papamoschou (1986). Up to the present time there is a lack of measured density profiles: the authors are unable to find any in the literature. The reason for the choice of (9) is its simplicity but it should be replaced by a more realistic distribution whenever such information becomes available.

Now consider a periodic Mach wave system generated by a slightly wavy bottom surface (with wavenumber  $k_M$ ) of the channel as shown in figure 4. To the right of the first Mach wave the wavy wall surfaces are given by the formula

Bottom wall 
$$y = -H_2 + \frac{2\pi\epsilon}{k_M}\sin{(k_M x)}, \tag{10} \label{eq:10}$$

Top wall 
$$y = H_1 + \frac{2\pi\epsilon\alpha}{k_M} \sin(k_M x + \phi). \tag{11}$$

It will be assumed that  $\epsilon$ , the ratio of the maximum vertical displacement of the bottom wavy wall to the wavelength, is much smaller than 1 (say no more than 1.5%):  $\epsilon$  being very small provides a natural parameter for perturbation analysis later. In figure 4 it is implied that the Mach wave system is generated by the bottom wall. The Mach wave system passes through the shear layer upward to reach the top wall where, for simplicity, a no-reflection condition is imposed. This is done by an appropriate choice of the amplitude and phase parameters  $\alpha$  and  $\phi$  of (11). In this way a well-defined periodic Mach wave system, except for the weak reflected wave

off the shear layer, is imposed on the confined supersonic shear layer. With  $\epsilon \ll 1$  a linear Mach wave solution will suffice. For clarity, we will use a subscript M to denote the physical variables associated with the Mach wave system. By linearizing (4)–(6) it is easy to find that the governing equation for the pressure,  $p_M$ , associated with the Mach wave is

$$\left(\frac{\overline{u}^2}{a^2} - 1\right) \frac{\partial^2 p_M}{\partial x^2} - \frac{\partial^2 p_M}{\partial y^2} + \frac{2}{\overline{u}} \frac{d\overline{u}}{dy} \frac{\partial p_M}{\partial y} + \frac{1}{\overline{\rho}} \frac{d\overline{\rho}}{dy} \frac{\partial p_M}{\partial y} = 0,$$
(12)

where  $a = (\gamma \bar{p}/\bar{\rho})^{\frac{1}{2}}$  is the speed of sound. The shear layer as given by (8) and (9) is effectively confined within the region  $-\delta < y < \delta$ ;  $\delta = 3\delta_{\omega}$ . Outside this region (12) can be integrated readily which, together with the boundary condition on the wavy wall, gives

$$p_{M} = \frac{\overline{\rho}_{1} \, \overline{u}_{1}^{2} \, 2\pi e \alpha}{(M_{1}^{2} - 1)^{\frac{1}{2}}} \cos \left(k_{M} \, x - k_{M} (M_{1}^{2} - 1)^{\frac{1}{2}} (y - H_{1}) + \phi\right) \quad (\delta \leqslant y \leqslant H_{1}), \tag{13}$$

$$p_{M} = \frac{\bar{\rho}_{2} \, \bar{u}_{2}^{2} \, 2\pi e}{(M_{2}^{2} - 1)^{\frac{1}{2}}} \cos{(k_{M} \, x - k_{M} (M_{2}^{2} - 1)^{\frac{1}{2}} (y + H_{2}))} \quad (-H_{2} \leqslant y \leqslant -\delta). \tag{14}$$

In addition to the Mach waves give by (14) there is also a weak reflected wave (off the shear layer) in the lower uniform region. The reflected wave solution is

$$p_{\rm R} = \beta \epsilon \cos(k_M x + k_M (M_2^2 - 1)^{\frac{1}{2}} y + \psi), \tag{15}$$

where  $\beta$  and  $\psi$  are as yet unknown constants.

To find the Mach wave solution inside the shear layer one may use (13) as the starting solution at  $y=\delta$  and integrate equation (12) until y=0 is reached. To simplify the integration, the cosine function in (10) can first be written in exponential form and the exp  $(ik_M x)$  and exp  $(-ik_M x)$  factors be separated out. Now one uses the linear combination of (14) and (15) as the starting solution at  $y=-\delta$  and integrates (12) up to y=0. Again the x-dependence in the form  $\exp(ik_M x)$  and  $\exp(-ik_M x)$  may be first separated out. The solutions are then joined at y=0. The requirements of continuity of solution and its first derivative provide four conditions by which the four unknowns  $\alpha$ ,  $\phi$ ,  $\beta$  and  $\psi$  can be determined.

# 3. Analysis of resonant instability by the method of multiple scales

We will now consider small-amplitude wave disturbances (denoted by a prime) superimposed on the mean flow and the periodic Mach wave system. Let

$$\begin{bmatrix} \rho \\ p \\ v \end{bmatrix} = \begin{bmatrix} \bar{\rho} \\ \bar{p} \\ \bar{v} \end{bmatrix} + \begin{bmatrix} \rho_M \\ p_M \\ v_M \end{bmatrix} + \begin{bmatrix} \rho' \\ p' \\ v' \end{bmatrix}.$$
mean Mach unsteady disturbance

To show the explicit dependence of the Mach waves on the small parameter  $\epsilon$  we will define

$$\begin{bmatrix} \rho_M \\ p_m \\ v_M \end{bmatrix} \equiv \epsilon \begin{bmatrix} \hat{\rho}_M \\ \hat{p}_M \\ \hat{v}_M \end{bmatrix}. \tag{17}$$

The governing equations for the unsteady disturbances can be found easily by substituting (16) into (4)–(6). To linear order these equations are

$$\frac{\partial \rho'}{\partial t} + \bar{u} \frac{\partial \rho'}{\partial x} + v' \frac{\mathrm{d}\bar{\rho}}{\mathrm{d}y} + \bar{\rho} \nabla \cdot v' = -\epsilon [\hat{v}_M \cdot \nabla \rho' + v' \cdot \nabla \hat{\rho}_M + \hat{\rho}_M \nabla \cdot v' + \rho' \nabla \cdot \hat{v}_M], \quad (18)$$

$$\begin{split} & \bar{\rho} \bigg[ \frac{\partial \boldsymbol{v}'}{\partial t} + \bar{u} \frac{\partial \boldsymbol{v}'}{\partial x} + v' \frac{\mathrm{d} \bar{u}}{\mathrm{d} y} \hat{\boldsymbol{e}}_x \bigg] + \boldsymbol{\nabla} p' \\ & = -\epsilon \bigg[ \hat{\rho}_M \frac{\partial \boldsymbol{v}'}{\partial t} + \bar{\rho} \hat{\boldsymbol{v}}_M \cdot \boldsymbol{\nabla} \boldsymbol{v}' + \hat{\rho}_M \, \bar{u} \frac{\partial \boldsymbol{v}'}{\partial x} + \hat{\rho}_M \, v' \frac{\mathrm{d} \bar{u}}{\mathrm{d} y} \hat{\boldsymbol{e}}_x + \bar{\rho} \boldsymbol{v}' \cdot \boldsymbol{\nabla} \hat{\boldsymbol{v}}_M + \rho' \bar{u} \frac{\partial \hat{\boldsymbol{v}}_M}{\partial x} + \rho' \hat{v}_M \frac{\mathrm{d} \bar{u}}{\mathrm{d} y} \hat{\boldsymbol{e}}_x \bigg], \end{split}$$

$$\frac{\partial p'}{\partial t} + \bar{u}\frac{\partial p'}{\partial x} + \gamma \bar{p}\nabla \cdot v' = -\epsilon[\hat{v}_M \cdot \nabla p' + v' \cdot \nabla \hat{p}_M + \gamma \hat{p}_M \nabla \cdot v' + \gamma p' \nabla \cdot \hat{v}_M], \quad (20)$$

where (u, v, w) are the velocity components in the (x, y, z)-directions. The linearized boundary conditions on the top, bottom and sidewalls are

$$v' = 2\pi\epsilon\alpha \left[\cos\left(k_M x + \phi\right)u' - \frac{1}{k_M}\sin\left(k_M x + \phi\right)\frac{\partial v'}{\partial y}\right] \quad \text{at} \quad y = H_1, \tag{21}$$

$$v' = 2\pi\epsilon \left[\cos\left(k_M x\right) u' - \frac{1}{k_M} \sin\left(k_M x\right) \frac{\partial v'}{\partial y}\right] \quad \text{at} \quad y = -H_2, \tag{22}$$

$$w' = 0$$
 at  $z = \pm \frac{1}{2}B$ . (23)

 $+ \gamma \hat{p}_{M} \nabla \cdot \boldsymbol{v}' + \gamma p' \nabla \cdot \hat{\boldsymbol{v}}_{M} \bigg| + O(\epsilon^{2}).$ 

#### 3.1. Multiple-scale expansion

Anticipating spatial resonant instability that occurs over distances of several wavelengths we will introduce a slow variable  $s = \epsilon x$ . With (x, y, z, s, t) as independent variables (18)–(20) become

$$\begin{split} \frac{\partial \rho'}{\partial t} + \overline{u} \frac{\partial \rho'}{\partial x} + v' \frac{\mathrm{d}\overline{\rho}}{\mathrm{d}y} + \rho' \nabla \cdot \mathbf{v}' \\ &= -\epsilon \left[ \overline{u} \frac{\partial \rho'}{\partial s} + \overline{\rho} \frac{\partial u'}{\partial s} + \hat{\mathbf{v}}_M \cdot \nabla \rho' + \mathbf{v}' \cdot \nabla \hat{\rho}_M + \hat{\rho}_M \nabla \cdot \mathbf{v}' + \rho' \nabla \cdot \hat{\mathbf{v}}_M \right] + O(\epsilon^2), \quad (24) \\ \overline{\rho} \left[ \frac{\partial \mathbf{v}'}{\partial t} + \overline{u} \frac{\partial \mathbf{v}'}{\partial x} + v' \frac{\mathrm{d}\overline{u}}{\mathrm{d}y} \hat{\mathbf{e}}_x \right] + \nabla p' \\ &= -\epsilon \left[ \overline{\rho} \overline{u} \frac{\partial \mathbf{v}'}{\partial s} + \frac{\partial p'}{\partial s} \hat{\mathbf{e}}_x + \hat{\rho}_M \frac{\partial \mathbf{v}'}{\partial t} + \overline{\rho} \hat{\mathbf{v}}_M \cdot \nabla \mathbf{v}' + \hat{\rho}_M \overline{u} \frac{\partial \mathbf{v}'}{\partial x} + \hat{\rho}_M v' \frac{\mathrm{d}\overline{u}}{\mathrm{d}y} \hat{\mathbf{e}}_x + \overline{\rho} \mathbf{v}' \cdot \nabla \hat{\mathbf{v}}_M \right. \\ &+ \rho' \overline{u} \frac{\partial \overline{\mathbf{v}}_M}{\partial x} + \rho' \hat{\mathbf{v}}_M \frac{\mathrm{d}\overline{u}}{\mathrm{d}y} \hat{\mathbf{e}}_x \right] + O(\epsilon^2), \quad (25) \\ \frac{\partial p'}{\partial t} + \overline{u} \frac{\partial p'}{\partial x} + \gamma \overline{p} \nabla \cdot \mathbf{v}' = -\epsilon \left[ \overline{u} \frac{\partial p'}{\partial s} + \gamma \overline{p} \frac{\partial u'}{\partial s} + \hat{\mathbf{v}}_M \cdot \nabla p' + \mathbf{v}' \cdot \nabla \hat{p}_M \right] \end{split}$$

We will seek a solution of the above equations in the form of a multiple-scale expansion with  $\epsilon$  as the small parameter:

$$\begin{bmatrix} \rho' \\ p' \\ \mathbf{v}' \end{bmatrix} = \begin{bmatrix} \rho_0 \\ p_0 \\ \mathbf{v}_0 \end{bmatrix} + \epsilon \begin{bmatrix} \rho_1 \\ p_1 \\ \mathbf{v}_1 \end{bmatrix} + \epsilon^2 \begin{bmatrix} \rho_2 \\ p_2 \\ \mathbf{v}_2 \end{bmatrix} + \dots$$
 (27)

Substitution of (27) into (24)–(26) and boundary conditions (21)–(23) we find upon partitioning terms according to powers of  $\epsilon$  the following system of equations:

Order  $\epsilon^{0}$   $\frac{\partial \rho_{0}}{\partial t} + \bar{u} \frac{\partial \rho_{0}}{\partial x} + v_{0} \frac{\mathrm{d}\bar{\rho}}{\mathrm{d}y} + \bar{\rho} \nabla \cdot \mathbf{v}_{0} = 0, \tag{28a}$ 

$$\bar{\rho} \left[ \frac{\partial v_0}{\partial t} + \bar{u} \frac{\partial v_0}{\partial x} + v_0 \frac{\mathrm{d}\bar{u}}{\mathrm{d}y} \hat{\boldsymbol{e}}_x \right] + \nabla p_0 = 0, \tag{28b}$$

$$\frac{\partial p_0}{\partial t} + \bar{u} \frac{\partial p_0}{\partial x} + \gamma \bar{p} \nabla \cdot \boldsymbol{v}_0 = 0, \qquad (28c)$$

$$y = H_1, \quad v_0 = 0, \tag{28d}$$

$$y = -H_2, \quad v_0 = 0, \tag{28e}$$

$$z = \pm \frac{1}{2}B, \quad w_0 = 0;$$
 (28f)

Order  $\epsilon$ 

$$\frac{\partial \rho_1}{\partial t} + \bar{u} \frac{\partial \rho_1}{\partial x} + v_1 \frac{\mathrm{d}\bar{\rho}}{\mathrm{d}y} + \bar{\rho} \nabla \cdot v_1 = I_0, \tag{29}$$

$$\bar{\rho} \left[ \frac{\partial \boldsymbol{v}_1}{\partial t} + \bar{\boldsymbol{u}} \frac{\partial \boldsymbol{v}_1}{\partial x} + v_1 \frac{\mathrm{d}\bar{\boldsymbol{u}}}{\mathrm{d}y} \hat{\boldsymbol{e}}_x \right] + \boldsymbol{\nabla} p_1 = \boldsymbol{J_0}, \tag{30}$$

$$\frac{\partial p_1}{\partial t} + \bar{u} \frac{\partial p_1}{\partial x} + \gamma \bar{p} \nabla \cdot v_1 = K_0, \tag{31}$$

$$y = H_1, \quad v_1 = 2\pi\alpha \bigg[\cos\left(k_M\,x + \phi\right)u_0 - \frac{1}{k_M}\sin\left(k_M\,x + \phi\right)\frac{\partial v_0}{\partial y}\bigg], \tag{32}$$

$$y = -H_2, \quad v_1 = 2\pi \left[ \cos(k_M x) u_0 - \frac{1}{k_M} \sin(k_M x) \frac{\partial v_0}{\partial y} \right],$$
 (33)

$$z = \pm \frac{1}{2}B, \quad w_1 = 0. \tag{34}$$

The non-homogeneous terms  $I_0$ ,  $J_0$ ,  $K_0$  are given by the terms inside the brackets on the right-hand sides of (24)–(26) with the primed quantities replaced by the order- $\epsilon^0$  solution. The order- $\epsilon^0$  problem defined by  $(28\,a$ –f) is identical to the small-amplitude normal mode problem of a two-dimensional mixing layer inside a rectangular channel (in the absence of the periodic Mach waves). This problem has been studied and analysed by the present authors (Tam & Hu 1989). It has been found that there are four families of wave solutions. Two of them, the  $A_{mn}$  and  $B_{mn}$  ( $m=0,1,2,\ldots;n=1,2,3,\ldots$ ) modes, are unstable waves. The other two families, the  $C_{mn}$  and  $D_{mn}$  modes, are neutral acoustic waves. Typical dispersion relation of these waves are given in figure 2.

Let us now consider two waves with the same angular frequency  $\omega$  and m number. Without loss of generality let them be a  $C_{mn}$  and  $D_{mn'}$  wave. We will denote the wavenumbers of these waves as  $k_C$  and  $k_D$  and identify their eigenfunctions by

subscripts C and D respectively. Suppose that these are the waves that we wish to drive to resonant instability. For this purpose we will choose the wavenumbers of the Mach wave system,  $k_M$ , to satisfy the resonance criterion

$$k_M = k_C - k_D. (35)$$

Because the problem is linear, a linear combination of the  $C_{mn}$  and  $D_{mn'}$  wave solutions is also a solution of (28). Thus let

$$\begin{bmatrix} \rho_0 \\ p_0 \\ v_0 \end{bmatrix} = A_C(s) \begin{bmatrix} \rho_C(y, z) \\ p_C(y, z) \\ v_C(y, z) \end{bmatrix} e^{i(k_C x - \omega t)} + A_D(s) \begin{bmatrix} \rho_D(y, z) \\ p_D(y, z) \\ v_D(y, z) \end{bmatrix} e^{i(k_D x - \omega t)}.$$
(36)

In (36)  $k_C$ ,  $k_D$  and the eigenfunctions are known from the solution of the  $\epsilon^0$  problem.  $A_C(s)$  and  $A_D(s)$  are the amplitudes of the  $C_{mn}$  and  $D_{mn'}$  waves. They are functions of the slow variable s. These wave amplitudes are unknown at this stage. In the following it will be shown through the mechanism of mutual forcing that they grow exponentially with s, leading to resonant instability.

## 3.2. Solvability condition and the growth rate of resonant instability

By substitution of (36) into the non-homogeneous terms of the order- $\epsilon$  problem it is easy to find that there are two types of terms which lead directly to spatial resonance. One group of terms resonates with the  $D_{mn'}$  wave. They come from the product terms of wave  $C_{mn}$  and the Mach wave system and also the s-derivative terms of the  $D_{mn'}$  wave. The product terms have  $x_-$ ,  $z_-$  and t-dependence of the form

$$\begin{bmatrix} \sin(2m\pi z/B) \\ \text{or} \\ \cos(2m\pi z/B) \end{bmatrix} e^{i(k_C x - \omega t)} e^{-ik_M x} = \begin{bmatrix} \sin(2m\pi z/B) \\ \text{or} \\ \cos(2m\pi z/B) \end{bmatrix} e^{i(k_D x - \omega t)}.$$
 (37)

Another group of terms resonates with the  $C_{mn}$  wave. They come from the product terms of the  $D_{mn'}$  wave and the periodic Mach waves and also the s-derivative terms of the  $C_{mn}$  wave. The product terms have x-, z- and t-dependence of the form

$$\begin{bmatrix} \sin(2m\pi z/B) \\ \text{or} \\ \cos(2m\pi z/B) \end{bmatrix} e^{i(k_D x - \omega t)} e^{-ik_M x} = \begin{bmatrix} \sin(2m\pi z/B) \\ \text{or} \\ \cos(2m\pi z/B) \end{bmatrix} e^{i(k_C x - \omega t)}.$$
 (38)

Taking into account the different types of non-homogeneous terms we will make use of the linearity of the  $\epsilon$ -order problem to divide the solution into a linear combination of several particular solutions. We will label the particular solution specifically for non-homogeneous terms with x-, z- and t-dependence in the form of (37) by a subscript D (they resonate with the  $D_{mn'}$  wave). Similarly we will label the particular solution specifically for non-homogeneous terms with x-, z- and t-dependence in the form of (38) by a subscript C (for resonating with the  $C_{mn}$  wave). Thus let

$$\begin{pmatrix} \rho_{1} \\ p_{1} \\ u_{1} \\ v_{1} \\ w_{1} \end{pmatrix} = \begin{pmatrix} \hat{\rho}_{D}(y, s) \cos(2\pi m z/B) \\ \hat{\rho}_{D}(y, s) \cos(2\pi m z/B) \\ \hat{u}_{D}(y, s) \cos(2\pi m z/B) \\ \hat{v}_{D}(y, s) \cos(2\pi m z/B) \\ \hat{v}_{D}(y, s) \cos(2\pi m z/B) \end{pmatrix} e^{i(k_{D}x - \omega t)} + \begin{pmatrix} \hat{\rho}_{C}(y, s) \cos(2\pi m z/B) \\ \hat{\rho}_{C}(y, s) \cos(2\pi m z/B) \\ \hat{u}_{C}(y, s) \cos(2\pi m z/B) \\ \hat{v}_{C}(y, s) \cos(2\pi m z/B) \\ \hat{v}_{C}(y, s) \sin(2\pi m z/B) \end{pmatrix} e^{i(k_{C}x - \omega t)} + \text{other particular solutions.}$$

$$(39)$$

On substitution of (39) into the  $\epsilon$ -order problem defined by (29)–(34) and separating out the x-, z- and t-dependence, it is straightforward to find that the functions  $\hat{\rho}_D$ ,  $\hat{p}_D$  and  $\hat{v}_D$  of (39) are given by the solution of the following non-homogeneous boundary-value problem:

$$-i\vec{\rho}(\omega - \bar{u}k_D)\,\hat{u}_D + \bar{\rho}\hat{v}_D\frac{\mathrm{d}\bar{u}}{\mathrm{d}y} + ik_D\,\hat{p}_D = I_{1D}(y,s),\tag{40}$$

$$-\mathrm{i}\bar{\rho}(\omega-\bar{u}k_D)\,\hat{v}_D + \frac{\mathrm{d}\hat{p}_D}{\mathrm{d}y} = I_{2D}(y,s), \tag{41}$$

$$-\operatorname{i}\!\overline{\rho}(\omega-\overline{u}k_{\scriptscriptstyle D})\,\hat{w}_{\scriptscriptstyle D}-\left(\!\frac{2\pi m}{B}\!\right)\!\hat{p}_{\scriptscriptstyle D}=I_{3D}(y,s), \tag{42}$$

$$-\mathrm{i}(\omega - \bar{u}k_D)\,\hat{p}_D + \gamma \bar{p} \bigg(\mathrm{i}k_D\,\hat{u}_D + \frac{\mathrm{d}\hat{v}_D}{\mathrm{d}y} + \frac{2\pi m}{B}\,\hat{w}_D\bigg) = I_{4D}(y,s), \tag{43}$$

$$\hat{v}_D = \beta_{1D} \quad \text{at} \quad y = H_1, \tag{44}$$

$$\hat{v}_p = \beta_{2p} \quad \text{at} \quad y = -H_2. \tag{45}$$

The non-homogeneous terms  $I_{1D}$ ,  $I_{2D}$ ,  $I_{3D}$ ,  $I_{4D}$ ,  $\beta_{1D}$  and  $\beta_{2D}$  which depend on the  $e^0$ -order solution are known functions of y. They also depend linearly on  $A_C$  and  $\mathrm{d}A_D/\mathrm{d}s$ . These functions can be found in a straightforward manner and, therefore, will not be written out explicitly.

Clearly the above non-homogeneous problem admits the  $D_{mn'}$  wave solution of (36) as an eigensolution, i.e.  $\hat{p}_D = p_D$ ,  $\hat{v}_D = v_D$  is a solution of the corresponding homogeneous problem. Thus by the Fredholm alternative theorem there is no solution to the problem unless the non-homogeneous terms satisfy the solvability condition. In other words, a bounded periodic solution in x exists only if the solvability condition is satisfied. By applying appropriate integration by parts it is easy to find from (40)–(45) that the solvability condition is

$$\int_{-H_{2}}^{H_{1}} \left[ I_{1D} k_{D} p_{D} + i I_{2D} \frac{\mathrm{d}p_{D}}{\mathrm{d}y} - i \left( \frac{2\pi m}{B} \right) I_{3D} p_{D} + \frac{\bar{\rho}}{\gamma \bar{p}} (\omega - \bar{u}k_{D}) I_{4D} p_{D} \right] \frac{\mathrm{d}y}{\bar{\rho}(\omega - \bar{u}k_{D})^{2}} - \frac{p_{D} \beta_{1D}}{(\omega - \bar{u}k_{D})} \Big|_{y=H_{2}} + \frac{p_{D} \beta_{2D}}{(\omega - \bar{u}k_{D})} \Big|_{y=-H_{2}} = 0. \quad (46)$$

For the acoustic modes considered here, the integrand is regular.

On carrying out the integration of (46) an equation relating the wave amplitudes  $A_{C}(s)$  and  $A_{D}(s)$  of (36) in the form

$$\mu_1 \frac{\mathrm{d}A_D}{\mathrm{d}s} + \nu_1 A_C = 0 \tag{47}$$

is obtained, where  $\mu_1$  and  $\nu_1$  are constants. Similar consideration for the non-homogeneous terms of the form of (38) provides an equation relating  $A_C(s)$  and  $A_D(s)$  in the form

$$\mu_2 \frac{\mathrm{d}A_C}{\mathrm{d}s} + \nu_2 A_D = 0. \tag{48}$$

The simultaneous solution of (47) and (48) is

$$\begin{bmatrix} A_C(s) \\ A_D(s) \end{bmatrix} = \begin{bmatrix} C_1 \\ C_2 \end{bmatrix} e^{\sigma s}, \tag{49}$$

$$\sigma = \pm \left(\frac{\nu_1 \nu_2}{\mu_1 \mu_2}\right)^{\frac{1}{2}} = \sigma_r + i\sigma_i. \tag{50}$$

With  $\sigma_{\rm r} > 0$  the  $C_{mn}$  and  $D_{mn'}$  waves will grow exponentially with s. The growth rate is proportional to  $\epsilon$ , i.e.

$$\frac{1}{|A_C|} \frac{\mathrm{d}|A_C|}{\mathrm{d}x} = \frac{1}{|A_D|} \frac{\mathrm{d}|A_D|}{\mathrm{d}x} = \epsilon \sigma_{\mathrm{r}}.$$
 (51)

Numerical results of  $\sigma_{\rm r}$  will be presented in the next section.

We would like to point out that in the above analysis we have chosen a  $C_{mn}$  and a  $D_{mn'}$  wave to be the resonant waves. Clearly the choice is quite arbitrary. It can be waves from any two different wave families or two different modes from the same wave family. All these possible combinations have been explored in our numerical calculations. These numerical results will be discussed in the next section.

#### 4. Numerical results

We will adopt the notation  $C_{mn}-D_{mn'}$  to indicate the family and the mode numbers of the two waves involved in our resonant instability calculation. The single most interesting quantity as far as mixing enhancement is concerned is the growth rate parameter  $\sigma_r H$  of (51). For a given  $\epsilon$ , which is the ratio of the maximum height of the wavy wall to the wavelength, the spatial growth rate of resonant instability over the distance of one channel height is equal to  $\epsilon\sigma_r H$ . In this section numerical results of  $\sigma_r H$  for different wave modes under different mixing-layer operating conditions will be reported. Figure 5 shows a typical set of results. Here the values of  $\sigma_r H$  as a function of non-dimensional wave frequency  $\omega H/\overline{u}_1$  for a number of twodimensional wave modes are provided. In the calculation the fast-stream Mach number,  $M_1$ , was taken to be 3.5 and the slow-stream Mach number,  $M_2$ , to be 1.2. The sound speed ratio  $(a_1/a_2)$  was set to be 1.2. In addition, the shear layer has been assumed to have a vorticity thickness to channel height ratio  $(\delta_{\omega}/H)$  of 0.05. As can be seen,  $\sigma_r H$  varies not only with frequency but also much more strongly with mode numbers. It appears that the growth rates of the lower-order modes are quite small. They are, therefore, not likely to be candidates for mixing enhancement purposes.

To provide an estimate of whether the resonant instability mechanism proposed in this paper is a viable scheme for mixing enhancement we are faced with the problem of not knowing what is the minimum growth rate required. At the present time, as far as we know, there is not enough experimental and theoretical understanding to offer any hint as to what it ought to be. This is not too surprising for even in the relatively well-researched subject of boundary-layer transition only semi-empirical criteria are available. One of these criteria which seems to have received general acceptance is the e<sup>9</sup>-amplification factor of Smith & Gamberoni (1956) (see also Reshotko 1976). The suggestion is that as an empirical rule one may assume that transition takes place after the Tollmien-Schlichting instability waves have amplified by e<sup>9</sup> folds. In the complete absence of any working formula we will adopt the same e<sup>9</sup> amplification factor as a mixing enhancement criterion. We are aware that this is arbitrary and has no sound justification. We can only hope that a more rational formula would become available in the future. Now for practical considerations we will restrict  $\epsilon$  to no more than  $1\frac{1}{2}\%$  and allow a distance of ten channel heights for amplification. With these specifications it is easy to find that  $\sigma_{\rm r}H$  must be greater than or equal to 60 in order to produce an e<sup>9</sup>-fold increase in

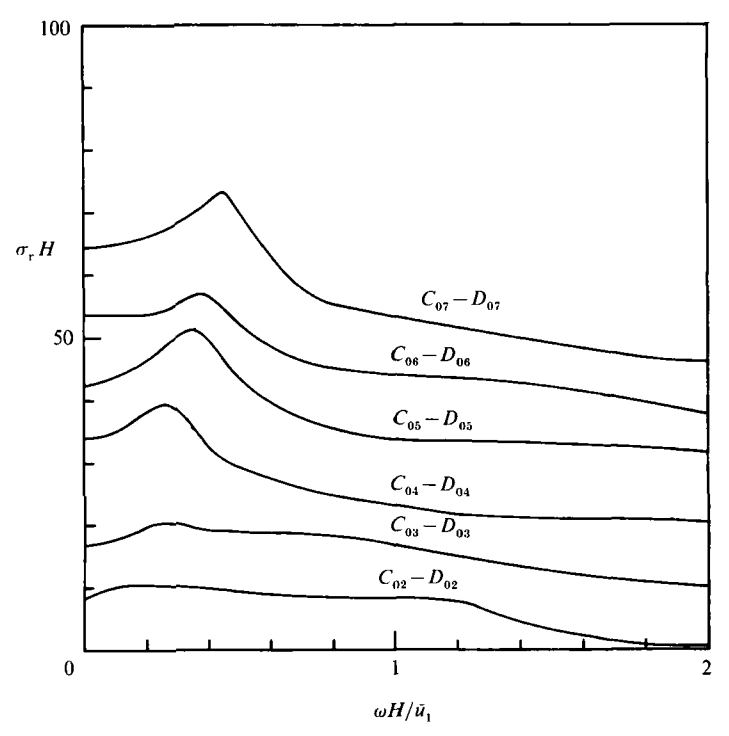


FIGURE 5. Dependence of resonant instability growth parameter  $\sigma_r H$  on non-dimensional frequency  $\omega H/\bar{u}_1$  (spatial growth rate  $= \epsilon \sigma_r H$ ) for different wave modes.  $M_1 = 3.5, M_2 = 1.2, a_1/a_2 = 1.2, H_1 = H_2, \gamma_1 = \gamma_2 = 1.4, \delta_w/H = 0.05.$ 

amplitude. Therefore, in the following we will be particularly interested in cases for which the resonant instability growth parameter  $\sigma_r H$  is greater than or close to 60.

To assess the effectiveness of using resonant instability for mixing enhancement under different operating conditions a parametric study has been carried out. The results of this study will now be reported.

#### 4.1. Wave mode effects

Figure 5 provides the dependence of the spatial resonant instability growth parameter  $\sigma_{\rm r}H$  on frequency for a number of  $C_{0n}-D_{0n}$  wave modes. It was pointed out above that there is latitude in choosing the resonant wave modes. Here several choices will be examined. Figure 6 illustrates the strong dependence of this parameter on the modal number and wave family. In figure 6(a) the growth rate parameter for  $C_{07}-D_{0n}$  (n=2,3,...,7) wave modes are given. It is clear from this figure that the resonant instability growth rate is generally smaller when the difference in the n-numbers of the two wave modes involved is larger. The numerical results appear to suggest that it is advantageous to keep the n-numbers the same in the selection of wave modes. Figure 6(b,c) shows that resonant instabilities associated with  $C_{0n}-B_{0n'}$ , and  $C_{0n}-A_{0n'}$  and  $D_{0n}-A_{0n'}$  wave modes are very ineffective. Based on these results we will limit our consideration to C-D modes in the rest of this paper.

4.2. Three-dimensional wave modes

Numerical values of the spatial resonant instability growth rate parameter typical of three-dimensional wave modes (m = 1) are shown in figure 7. The mean flow conditions are the same as in figure 5. By comparing these two figures it is easy to

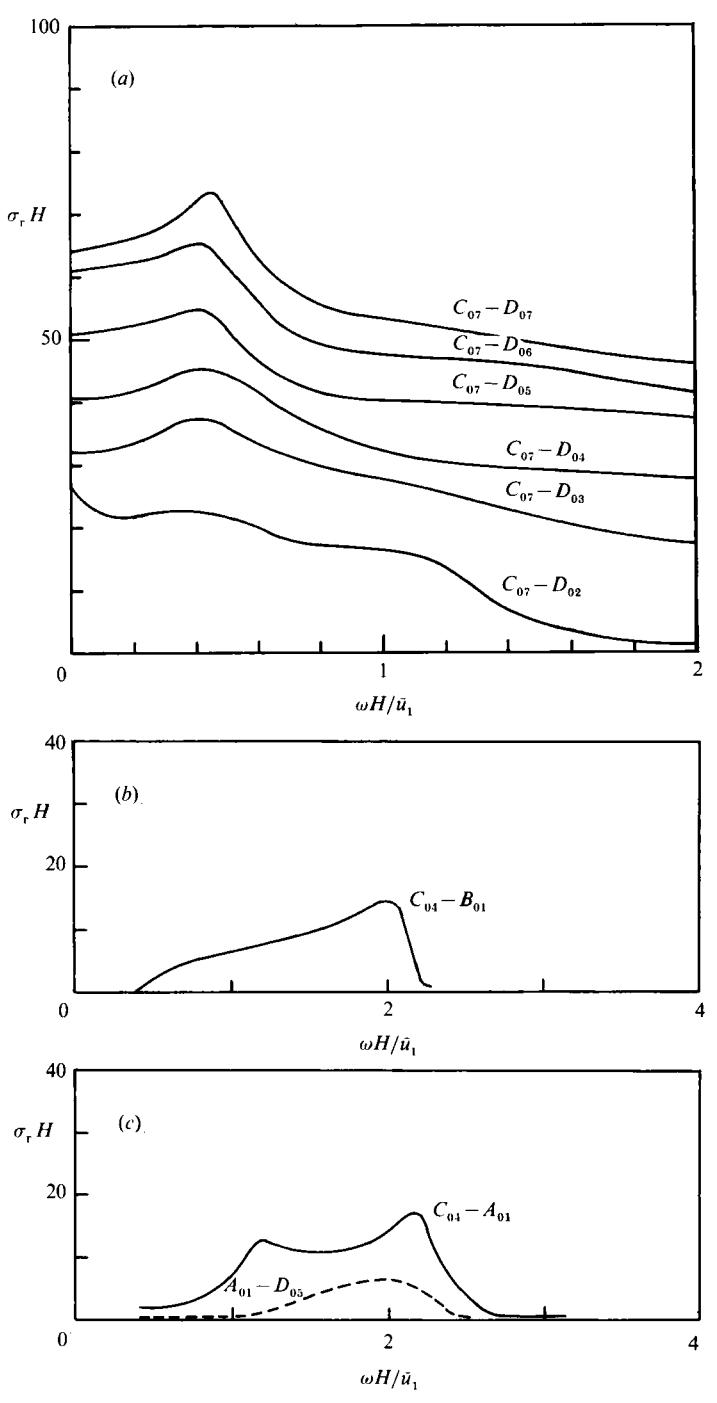


Figure 6. Dependence of resonant instability growth parameter  $\sigma_{\rm r} H$  on wave modes. (a)  $C_{\rm 07}-D_{\rm 0n}$  wave modes (n = 2, 3, ..., 7). (b)  $C_{\rm 04}-B_{\rm 01}$ , (c)  $C_{\rm 04}-A_{\rm 01}$  and  $A_{\rm 01}-D_{\rm 05}$ .

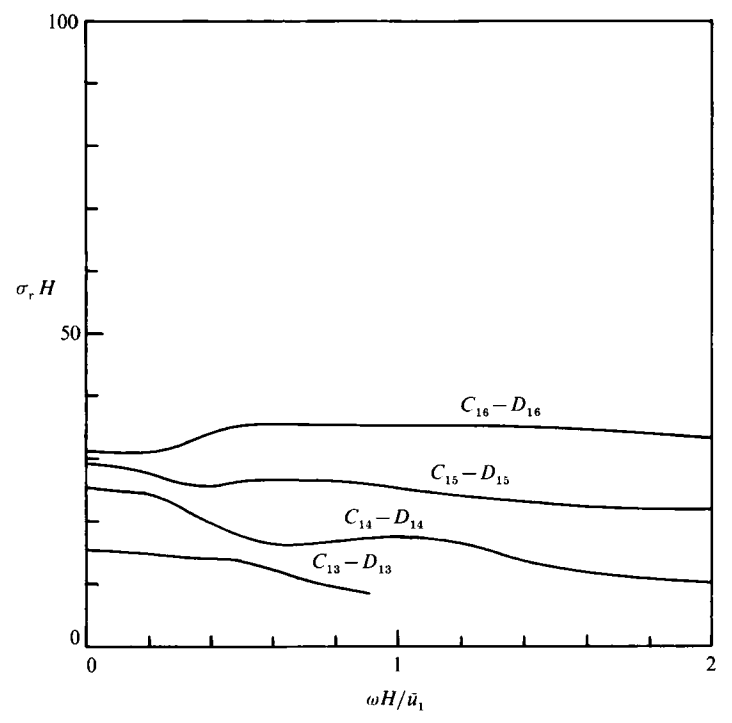


FIGURE 7. Growth parameter  $(\sigma_r H)$  for three-dimensional wave modes (m=1).  $M_1=3.5, M_2=1.2, a_1/a_2=1.2, \gamma_1=\gamma_2=1.4, \delta_w/H=0.05, H_1=H_2, B=H.$ 

see that two-dimensional wave modes generally have higher growth rates. Since our aim is to find conditions with the highest growth rate we will confine our attention to two-dimensional wave modes.

#### 4.3. Effects of shear-layer thickness

It is well known that the thickness of a mixing layer exerts great influence on the growth rate of its natural instability waves. An example is given in figure 3. For the  $A_{01}$  instability wave mode the maximum growth rate decreases by over 50% as the thickness increases from  $\delta_{\omega}/H=0.05$  to 0.2. In fact, it is this tendency of rapid decrease in growth rate with increase in mixing-layer thickness which effectively limits the natural mixing rate of shear layers especially at supersonic speeds. Figure 8(a) shows the dependence of the growth rate parameter of resonant instability on shear-layer thickness at frequency  $\omega H/\bar{u}_1=1.0$ . Figure 8(b) shows a similar dependence at  $\omega H/\bar{u}_1=0.4$ . Contrary to expectation  $\sigma_{\rm r}H$  does not seem to be affected by changes in shear-layer thickness at all. This is true for all the wave modes we have considered. This result is most useful for estimating the total growth of the instability since the downstream changes in growth rate can be effectively ignored.

### 4.4. Effects of Mach number

Our computational study on the spatial growth parameter  $(\sigma_r H)$  of resonant instability indicates that it is very much affected by the flow Mach numbers. Figure 9 is a plot of this parameter for the  $C_{06}-D_{06}$  wave modes at a slow-stream Mach number of 1.2 as the fast-stream Mach number,  $M_1$ , varies. At low  $M_1$  the growth parameter is very large. As  $M_1$  increases  $\sigma_r H$  decreases monotonically. For  $M_1$  greater

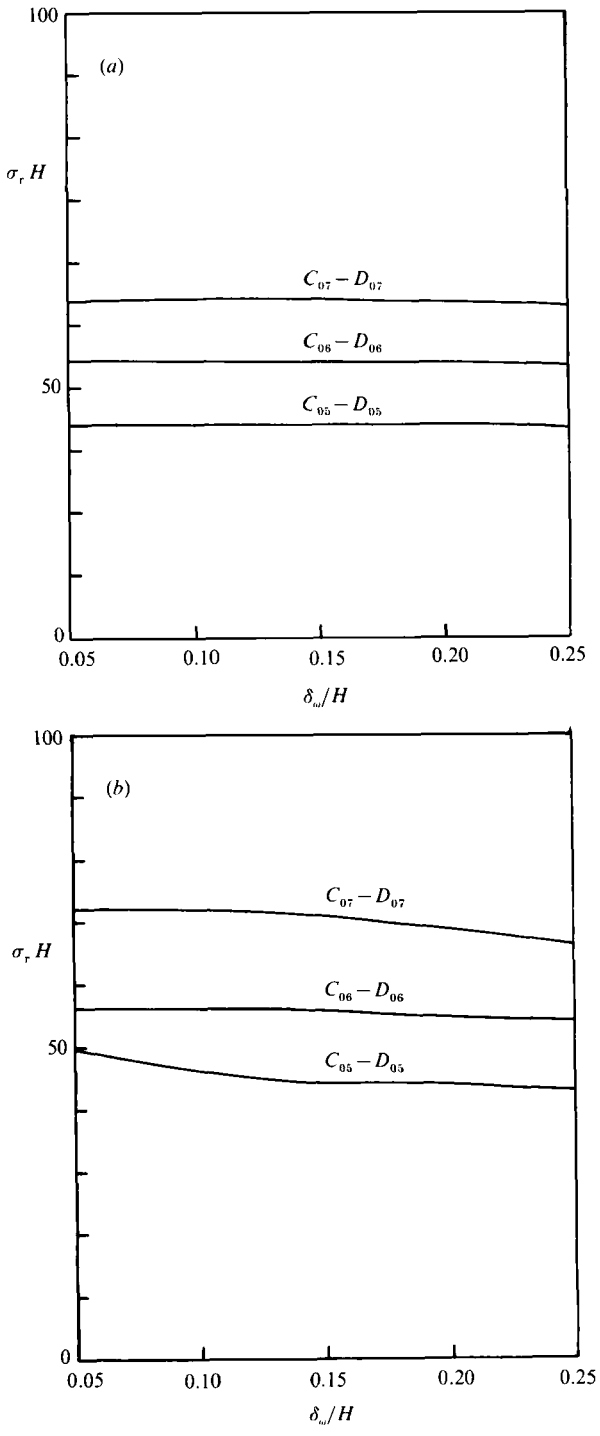


FIGURE 8. Effect of mixing-layer thickness on the spatial growth rate parameter  $\sigma_r H$  at a fixed frequency.  $M_1=3.5,\,M_2=1.2,\,a_1/a_2=1.2,\,\gamma_1/\gamma_2=1.4.$  (a)  $\omega H/\bar{u}_1=1.0,$  (b)  $\omega H/\bar{u}_1=0.4.$ 

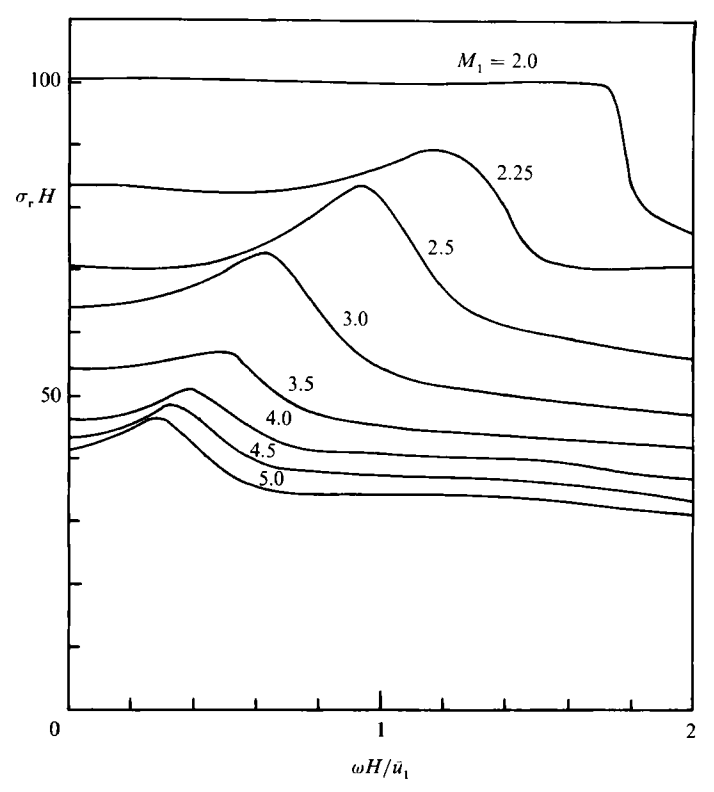
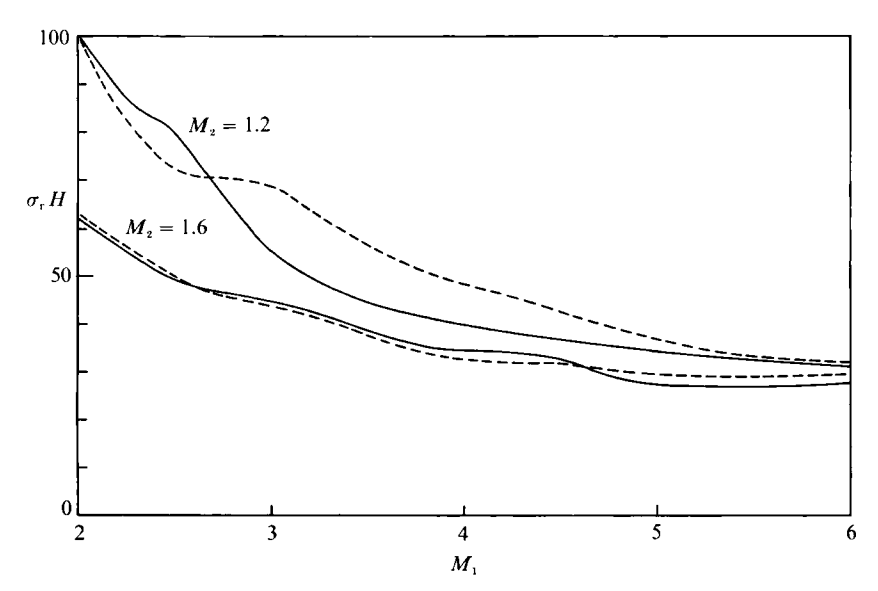


Figure 9. Dependence of spatial growth rate parameter  $\sigma_{\rm r}H$  on  $M_1$  for the  $C_{06}-D_{06}$  wave modes.  $M_2=1.2,\,a_1/a_2=1.0,\,\gamma_1=\gamma_2=1.4,\,\delta_{\omega}/H=0.05.$ 



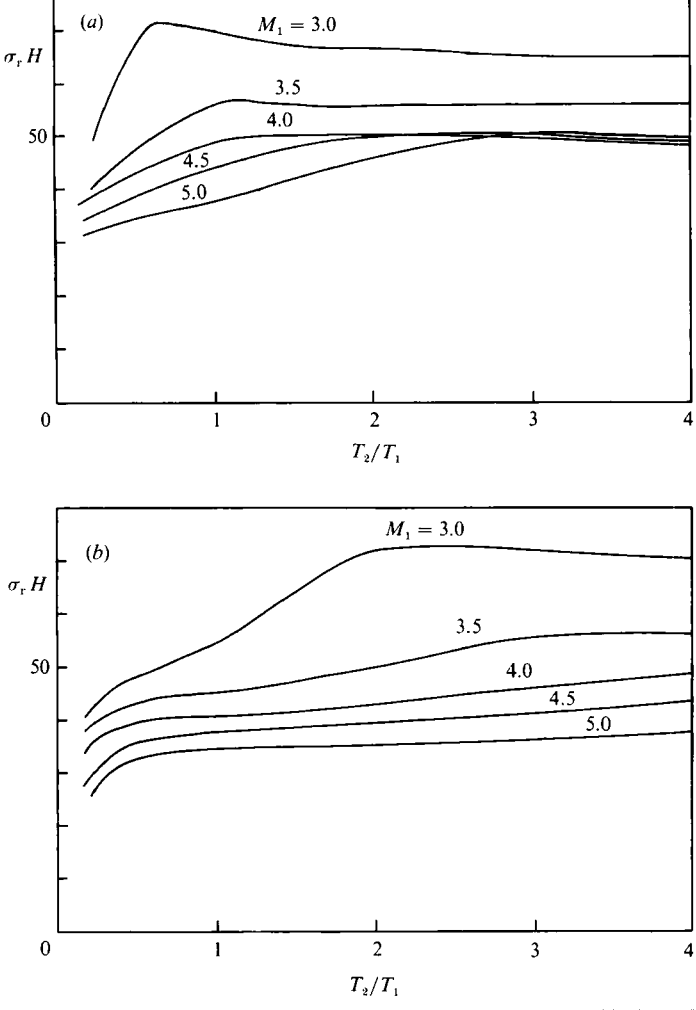


FIGURE 11. Effect of temperature on spatial growth parameter  $\sigma_r H$ .  $C_{06} - D_{06}$  wave modes.  $M_2 = 1.2, \ \gamma_1 = \gamma_2 = 1.4. \ (a) \ \omega H/\bar{u}_1 = 0.5. \ (b) \ \omega H/\bar{u}_1 = 1.0.$ 

than 3.0 there is only a narrow range of frequencies for which  $\sigma_{\rm r}H$  is close to 60. In other words, resonant instability as a mixing enhancement mechanism becomes less and less effective with increasing Mach numbers. Figure 10 shows the effect of increasing  $M_2$  as well as  $M_1$  at fixed frequencies. As can be seen, at moderate Mach number  $M_1$  a small increase in  $M_2$  can lead to a large reduction in growth rate. Based on the values of this figure it appears that if the resonant instability mechanism is to be useful the Mach number of the slow stream must be in the low supersonic range.

## 4.5. Effects of temperature

Here we consider the effect of heating the slow stream on the growth rate parameter  $\sigma_{\rm r}H$ . Figure 11(a) at  $\omega H/\bar{u}_1=0.5$  shows that, regardless of Mach numbers, heating of the slow stream generally increases  $\sigma_{\rm r}H$ . This temperature effect, however, becomes saturated at high temperature ratio. Figure 11(b) at  $\omega H/\bar{u}_1=1.0$  shows similar trends. At higher frequency it seems that the effect can be realized over a large range of temperature ratios. Figure 12 shows the effect of heating over the

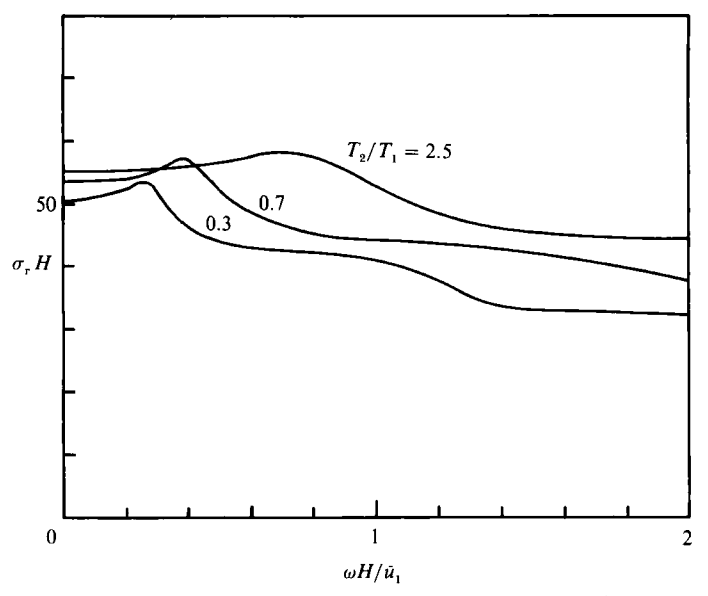


Figure 12. Effect of heating of the slow stream on the spatial growth parameter  $\sigma_{\rm r}H$ .  $C_{\rm 06}-D_{\rm 06}$  wave modes.  $M_1=3.5,~M_2=1.2,~\gamma_1=\gamma_2=1.4,~\delta_{\rm w}=0.05.$ 

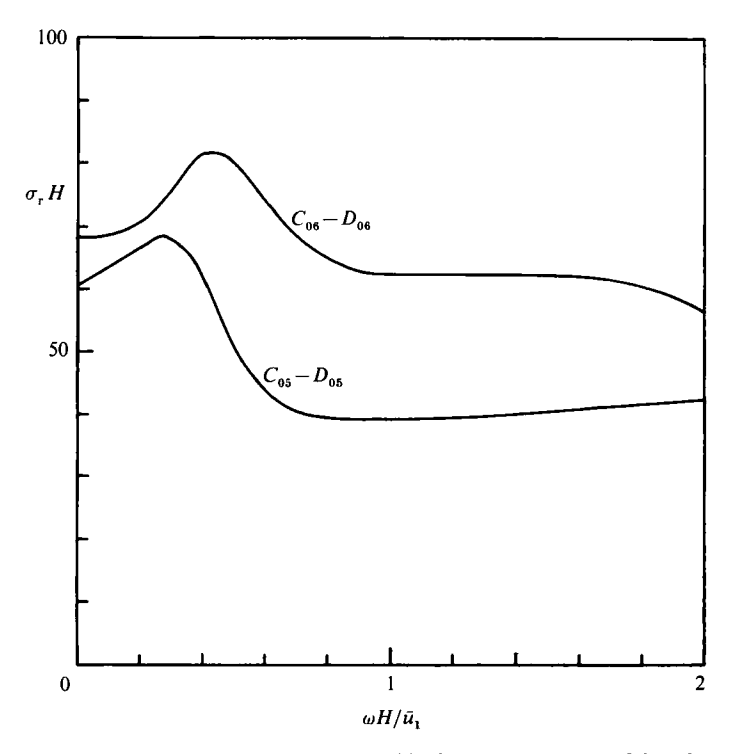


Figure 13. Spatial growth parameter. Mach waves generated by the top wall.  $M_1=3.5,\,M_2=1.2,\,a_1/a_2=1.2,\,\gamma_1=\gamma_2=1.4,\,\delta_\omega/H=0.05,\,H_1=H_2,\,m=0.$ 

range of frequency up to  $\omega H/\bar{u}_1=2.0$ . A careful examination of the computed results reveals that the growth parameter appears to peak at  $\omega/k_r=\bar{u}_2-a_2$ . As  $T_2/T_1$  increases  $(\bar{u}_2-a_2)$  increases also. Therefore, the peak of  $\sigma_r H$  moves to the right with increase in  $T_2/T_1$ . It is safe to say that heating the slow stream while keeping the Mach numbers fixed generally makes the resonant instability growth rate increase. On the other hand, the opposite is true when heating is applied to the fast stream.

To conclude this section we would like to point out that so far it has been assumed that the Mach wave system is generated by the lower wall (see figure 4) and cancelled by an appropriate choice of the amplitude and phase of the wavy upper surface. It is, of course, possible to reverse the role of the top and bottom walls. Figure 13 shows calculated results for flow conditions identical to those of figure 5 except that the Mach wave system is generated by the top wall. On comparing figures 5 and 13 it is seen that the growth rates given in figure 13 is higher than the corresponding values in figure 5. However, it must be pointed out that for the same  $\varepsilon$  the Mach waves generated by the top wall are stronger; it being adjacent to the faster stream. With this in mind it is probably not worthwhile making detailed comparisons between the two Mach wave arrangements. The important point to note is that there is more than one way to introduce the periodic Mach wave system.

#### 5. Discussion

In this paper we have demonstrated that it is possible to induce resonant instability involving two natural wave modes of a supersonic shear layer inside a rectangular channel by a periodic Mach wave system. The periodic Mach waves do not supply energy to the resonant waves. They act as catalysts. Their presence allows the two natural wave modes to exert secular forcing on each other. The simultaneous mutual forcing gives rise to spatial growth. The spatial growth rate of the resonant instability can be quite large. To provide an idea of its magnitude, if we take  $\epsilon = 0.015$  and  $\sigma_r H = 60$  then the growth rate over the distance of a channel height is 0.9. For comparison, the maximum growth rate of the natural instability wave under typical flow conditions as given in figure 3 is about 0.5 per channel height (taking  $\delta_\omega/H = 0.08$ ) and becomes much smaller as the thickness of the shear layer increases. Thus resonant instability is potentially a more powerful mechanism for mixing enhancement than the excitation of the natural instability waves.

So far one aspect of using the periodic Mach wave system has not been discussed: the performance loss due to increase in drag. First of all with supersonic flow there is a wave drag. It is a simple matter to show that the wave drag is proportional to  $\epsilon^2$ , so with small  $\epsilon$  this loss is relatively small. However, there will also be an added viscous drag due to the wavy surface. For high-temperature, high-speed flow we do not have a simple formula for estimating the added viscous drag. We believe that it is probably of the same order of magnitude as the wave drag. If this is the case the total drag might not be of great significance overall.

This work was supported by the office of Naval Research under Grant No. N00014-87-J-1130 and also in part by the Florida State University through time granted on its ETA-10 supercomputer. The authors would like to thank the careful reviewing of the referees and their excellent suggestions for improving this paper.

#### REFERENCES

- Bogdanoff, D. W. 1983 Compressible effects in turbulent shear layers. AIAA J. 21, 926-927.
- CHINZEI, N., MASUYA, G., KOMURO, T., MURAKAMI, A. & KUDEN, K. 1986 Spreading of two-stream supersonic turbulent mixing layers. *Phys. Fluids* 29, 1345-1347.
- Greenough, J. A., Riley, J. J., Soetrisbmno, M. & Eberhardt, D. S. 1989 The effects of walls on a compressible mixing layer. AIAA Paper 89-0372.
- IKAWA, H. & KUBOTA, T. 1975 Investigation of supersonic turbulent mixing with zero pressure gradient. AIAA J. 13, 566-572.
- Jackson, T. L. & Grosch, C. E. 1989 Absolute/convective instabilities and the convective Mach number in a compressible mixing layer. *ICASE Rep.* 89-38.
- Mei, C. C. 1985 Resonant reflection of surface water waves by periodic sandbars. J. Fluid Mech. 152, 315–335.
- Mei, C. C., Hara, T. & Naciri, M. 1988 Note on Bragg scattering of water waves by parallel bars on the seabed. J. Fluid Mech. 186, 147-162.
- Mack, L. M. 1989 On the inviscid acoustic-mode instability of supersonic shear flows. Proc. Fourth Symp. on Numer. and Phys. Aspects of Aerodyn. Flows.
- MILES, J. W. 1958 On the disturbed motion of a plane vortex sheet. J. Fluid Mech. 4, 538-552.
- Nayfeh, A. H. 1973 Perturbation Methods. Wiley-Interscience.
  Papamoschou, D. 1986 Experimental investigation of heterogeneous compressible shear layers.
- Ph.D. thesis, California Institute of Technology.

  Papamoschou, D. & Roshko, A. 1986 Observations of supersonic free shear layers. AIAA Paper
- 86-0162. Рарамовской, D. & Roshko, A. 1988 The compressible turbulent shear layers: an experimental
- study. J. Fluid Mech. 197, 453-477.

  RAGAB, S. A. & Wu, J. L. 1989 Linear instabilities in two-dimensional compressible mixing
- layers. Phys. Fluids A 1, 957-966. Reshotko, E. 1976 Boundary-layer stability and transition. Ann. Rev. Fluid Mech. 8, 311-349.
- Smith, A. M. O. & Gamberoni, N. 1956 Transition, pressure gradient and stability theory.

  Douglas Aircraft Company (El Segundo) Rep. ES 26388.
- T<sub>AM</sub>, C. K. W. & Hu, F. Q. 1989 The instability and acoustic wave modes of supersonic mixing layers inside a rectangular channel. *J. Fluid Mech.* 203, 51-76.
- Zhuang, M., Kubota, T. & Dimotakis, P. E. 1988 On the instability of inviscid compressible free shear layers. AIAA Paper 88-3538.
- Zhuang, M., Kubota, T. & Dimotakis, P. E. 1990 The effect of walls on a spatially growing supersonic shear layer. *Phys. Fluids* A 2, 599-604.